IOP Publishing Superconductor Science and Technology
Supercond. Sci. Technol. **28** (2015) 095009 (8pp) doi:10.1088/0953-2048/28/9/095009

Ti-doping effects on magnetic properties of dense MgB_2 bulk superconductors

Tomoyuki Naito, Takafumi Yoshida and Hiroyuki Fujishiro

Faculty of Engineering, Iwate University, Morioka 020-8551, Japan

E-mail: tnaito@iwate-u.ac.jp

Received 4 June 2015, revised 22 June 2015
Accepted for publication 25 June 2015
Published 27 July 2015

Abstract

We have studied the effects of Ti doping on the magnetic properties of MgB_2 superconducting bulks. The trapped field, which was obtained by field-cooled magnetization, B_T^{FC}, was about 3.6 T at 13 K at the surface of the single Ti5–20% doped MgB_2 bulks, which was about 1.3 times larger than that of the non-doped bulk. The B_T^{FC} of 4.6 T was achieved at 14.1 K in the centre of the doubly stacked Ti-doped MgB_2 bulks. The remanent magnetic flux density, which corresponds to the trapped field by zero-field cooled magnetization, B_T^{ZFC}, was comparable with the absolute value of coercive force with a very small vortex creep rate of about 2% over 40 h. These results suggested that the MgB_2 bulk was an excellent 'quasi-permanent' magnet. The critical current density, J_c, under magnetic field was also enhanced by Ti doping; under 3 T at 20 K, the J_c of 4.0×10^3 A cm^{-2} for the pristine sample was enhanced to that of $1.6–1.8 \times 10^4$ A cm^{-2} for the Ti-doped samples. The irreversibility field exceeded 5 T at 20 K for the Ti-doped samples. The existence of nanometric unreacted B and strongly Mg-deficient Mg-B particles and TiB_2 layers at the periphery of Ti precipitates was suggested in the Ti-doped bulks by microscopic observation. The improvement of the vortex pinning properties in Ti-doped MgB_2 originated from the creation of the nanometric nonsuperconducting particles and TiB_2 layers acting as strong vortex pinning centres.

Keywords: MgB_2, superconducting bulk magnet, Ti-doping

1. Introduction

A quasi-permanent magnet using a superconducting bulk can be realized by vortex pinning, which is one of the specific features of type II superconductors. It has been intensively studied using melt-processed, single-grain RE-Ba-Cu-O (RE: rare earth element) bulks [1, 2], because the bulk can trap a magnetic field, B_T, of several Tesla at 77 K [3] and over 17 T below 30 K [4, 5]. Although the critical temperature, T_c, of MgB_2 [6] is much lower than that of RE-Ba-Cu-O bulks, it has a nature of weak-link-free grain boundaries [7, 8]. Therefore, we can study 'polycrystalline' MgB_2 bulk magnets, contrary to the RE-Ba-Cu-O melt-textured bulk.

In 2003, just after the discovery of MgB_2, Tesla-class MgB_2 bulk magnets were already reported by two groups [9, 10]. An MgB_2 bulk with 30 mm diameter, which was fabricated by a spark plasma sintering method under a pressure of 30 MPa, showed a critical current density of 10^5 A cm^{-2} and trapped a magnetic field of 1 T at 27.5 K [9]. Although a higher trapped field was expected at lower temperatures, the quench phenomenon occurred. A trapped field over 2 T was successfully achieved at 6 K using an MgB_2 bulk (28 mm in diameter) synthesized under a pressure of 2 GPa [10]. Recently, research on MgB_2 bulk magnets has come into the spotlight again [11–14], because it is rare-earth free and light weight, in addition to weak-link-free, which makes them suitable for industrial applications, such as magnetically levitated trains, wind power generators, and so on [15]. We have reported that the trapped field was improved by densification, from 1.5 T for the MgB_2 bulk (the filling factor, f, was about 50%) fabricated by the capsule method under an ambient pressure [11], to 2.5 T for the bulk (f was higher than 90%) fabricated by a hot isostatic pressing (HIP) method under a pressure of 98 MPa [12]; the HIP method has been used to densify MgB_2 in many works [6, 16, 17]. The densification by pressure sintering results in an increase in the number of grain boundaries, which are well known to act as vortex pinning centres, and at the same time, an increase in the cross section of the supercurrent path. As a

result, the critical current density and the trapped field were enhanced. Recently, a trapped field of 5.4 T at 12 K was achieved in a uniaxially hot pressed MgB_2 bulk using ball-milled nanometre-size powder [13], in which the concurrent densification and the grain-size refining were quite effective to enhance the trapped field.

Another approach to enhance the trapped field is to introduce the vortex pinning centres artificially. Chemical doping, such as Ti [18, 19] and C [20], was reported to improve the vortex pinning properties in MgB_2. In the $Mg_{1-x}Ti_xB_2$ (x = 0, 0.1, 0.2) samples fabricated under ambient pressure, the x = 0.1 sample showed a critical current density of 10^6 A cm^{-2} in the self-field at 20 K, which was about three orders of magnitude larger than that of the pristine (x = 0) sample and equivalent to that obtained for the pressure-sintered undoped samples [10, 21]. However, the J_c of the x = 0.2 sample degraded to approximately 10^5 A cm^{-2} under the same conditions. Therefore, x = 0.1 was reported to be the optimal Ti-doping level, which was also supported by other work [22]. Transmission electron microscope (TEM) analysis suggested that Ti was not substituted for either the Mg- or B-sites but created a thin TiB_2 layer between MgB_2 grain boundaries with nanometre-size, and the TiB_2 layer prevented the growth of MgB_2 grains. Furthermore, TiB_2 kept the connection between the MgB_2 grains, because it has the same crystal structure as MgB_2 and suppressed the creation of MgB_4, which usually deteriorates the connectivity. Therefore, Ti doping offers high connectivity with fine grains, resulting in high J_c values [18, 19]. In this paper, to achieve higher J_c and B_T values, Ti-doped MgB_2 bulks with three different Ti contents are prepared by the HIP method. We discuss the effect of Ti doping on the vortex pinning properties from the measurements of J_c and B_T and microscopic observations.

2. Experimental procedure

MgB_2 bulks were fabricated by an *in-situ* HIP method [6, 12, 16, 17]. The precursors were prepared as follows. Raw powders of Mg (99% in purity, $\leqslant$180 μm in grain size, Kojundo Chemical Laboratory Co., Ltd.), Ti (99% in purity, $\leqslant$ 45 μm in grain size, Kojundo Chemical Laboratory Co., Ltd.), and amorphous B (99% in purity, $\leqslant$46 μm in grain size, Furuuchi Chemical Corp.) were weighted with Mg:Ti:B = $(1-x)$:x:2.0 (x = 0, 0.05, 0.1, and 0.2) in molar ratio and ground well using an agate mortar and pestle. The mixed powder was pressed into pellets of 40 mm in diameter and 20 mm in thickness under a uniaxial pressure of about 12 MPa, and subsequently the pellet was further densified by a cold isostatic pressing method under the pressure of 196 MPa. The obtained precursor pellet was sealed in a stainless steel container in a vacuum by electron beam welding. The MgB_2 precursor in the container was sintered at 900° C for 3 h under an Ar-gas pressure of 98 MPa in the HIP furnace and cooled down to room temperature by furnace cooling. Disc-shaped MgB_2 bulks of about 38 mm diameter and 6.9 mm thickness were prepared by dry machining.

The MgB_2 bulk samples were magnetized by field cooling (FC) in a magnetic field of 5–8 T, applied parallel to the thickness direction using a 10 T cryogen-free superconducting magnet (JMTD-10T100, Japan Superconductor Technology (JASTEC), Inc.), and the applied magnetic field was then decreased to 0 T at a rate of 0.022–0.22 T/min. The bulks were placed on the cold stage of a Gifford–McMahon type helium refrigerator by inserting a thin In sheet to obtain good thermal contact. The trapped field was measured by a cryogenic Hall sensor (BHT-921, F.W. Bell, Inc.) mounted on the centre of the bulk surface using GE7031 varnish. The temperature of the bulk was monitored by a Cernox thermometer, which was adhered beside the Hall sensor on the bulk surface. After the FC magnetization, the superconducting properties, such as the critical temperature, T_c, and the critical current density, J_c, were evaluated using a small piece cut from the bulk. The magnetization, M, was measured as functions of temperature and magnetic field using a commercial SQUID magnetometer (MPMS-XL, Quantum Design, Inc.). The J_c was estimated from the magnetic hysteresis using the extended Bean model [23, 24]: $J_c = 20\Delta M/a(1 - a/3b)$, where ΔM is the width of the hysteresis, and a and b ($a < b$) are the cross-sectional dimensions of the sample perpendicular to the applied magnetic field. The microstructure and composition were analyzed by an electron probe micro-analyzer with a field-emission electron gun (FE-EPMA).

3. Results and discussion

Figure 1(a) shows the temperature dependence of the trapped magnetic field, $B_T(T)$, of the MgB_2 bulks with varying Ti content. The B_T value of the pristine bulk is about 2.5 T at the lowest temperature of 16 K, decreases with increasing temperature, and finally reaches zero at around 39 K. The B_T value is enhanced obviously by the Ti doping; the highest B_T value of the Ti5% bulk is about 3.6 T at 13.4 K, which is 1.3 times larger than the extrapolated value of 2.7 T for the pristine bulk. However, further doping does not provide higher B_T; the $B_T(T)$ curves of both Ti10 and Ti20% bulks are almost the same as that of the Ti5% bulk. Figure 1(b) shows the B_T value at 20 K as a function of Ti content. B_T increases from 2.2 T of the pristine bulk to a nearly constant value of 2.8 T for all the Ti-doped bulks. The temperature at which the B_T value became negligible was about 39 K for all the Ti-doped bulks, similar to the pristine bulk. The inset of figure 1(a) shows the temperature dependence of the reduced magnetization, $m(T)$(= $M(T)/M$(5 K)), of the pristine and Ti-doped samples under a magnetic field of 4 mT after zero-field cooling (ZFC). All the $m(T)$ curves are collapsed into the universal curve, and T_c is determined to be about 39 K for all the samples. These results suggest that no Mg site substitution by Ti took place, because this site substitution deteriorates T_c in general.

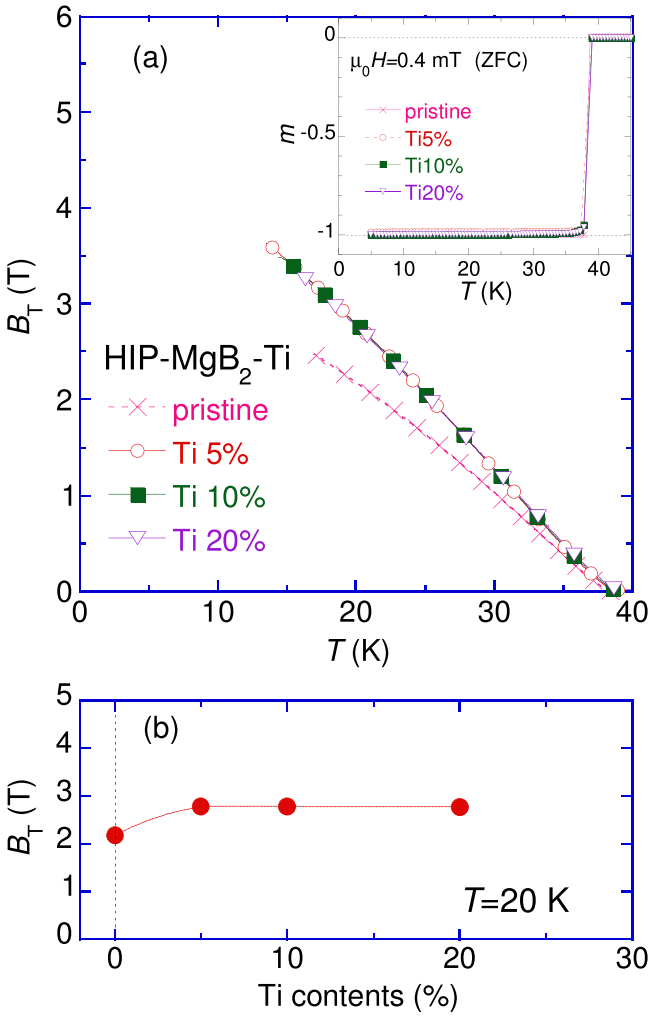

Figure 1. (a) Temperature dependence of the trapped magnetic field for the pristine and three Ti-doped MgB_2 bulks. Inset shows temperature dependence of the reduced magnetization at $\mu_0 H$ = 4 mT after zero-field cooling. (b) The trapped field at 20 K as a function of Ti contents.

We also examined the trapped field properties of doubly stacked bulks. Figure 2(a) shows the temperature dependence of B_T at the centre and the top surface of the stacked bulks, which consist of the lower Ti5% and the upper Ti10% bulks with a thin indium sheet between them, as depicted schematically in the inset of figure 2(a). The $B_T(T)$ curve of the single Ti10% bulk shown in figure 1(a) is also depicted for reference. The highest B_T values of 4.6 T at 14.1 K and 3.2 T at 16.3 K are achieved, respectively, for the centre and surface positions. The difference in the temperature between the positions comes from the influence of radiation loss and/or the temperature drop due to thermal contact resistance between the bulks. Although the surface B_T of the stacked bulks almost corresponds to that of the single Ti10% bulk, the centre B_T value is about 1.3 times larger than B_T at the surface bulk. These results suggest that the thicker bulk is not so effective for the enhancement of B_T at the surface, which is supported by our simulation results [25, 26], but a higher magnetic field

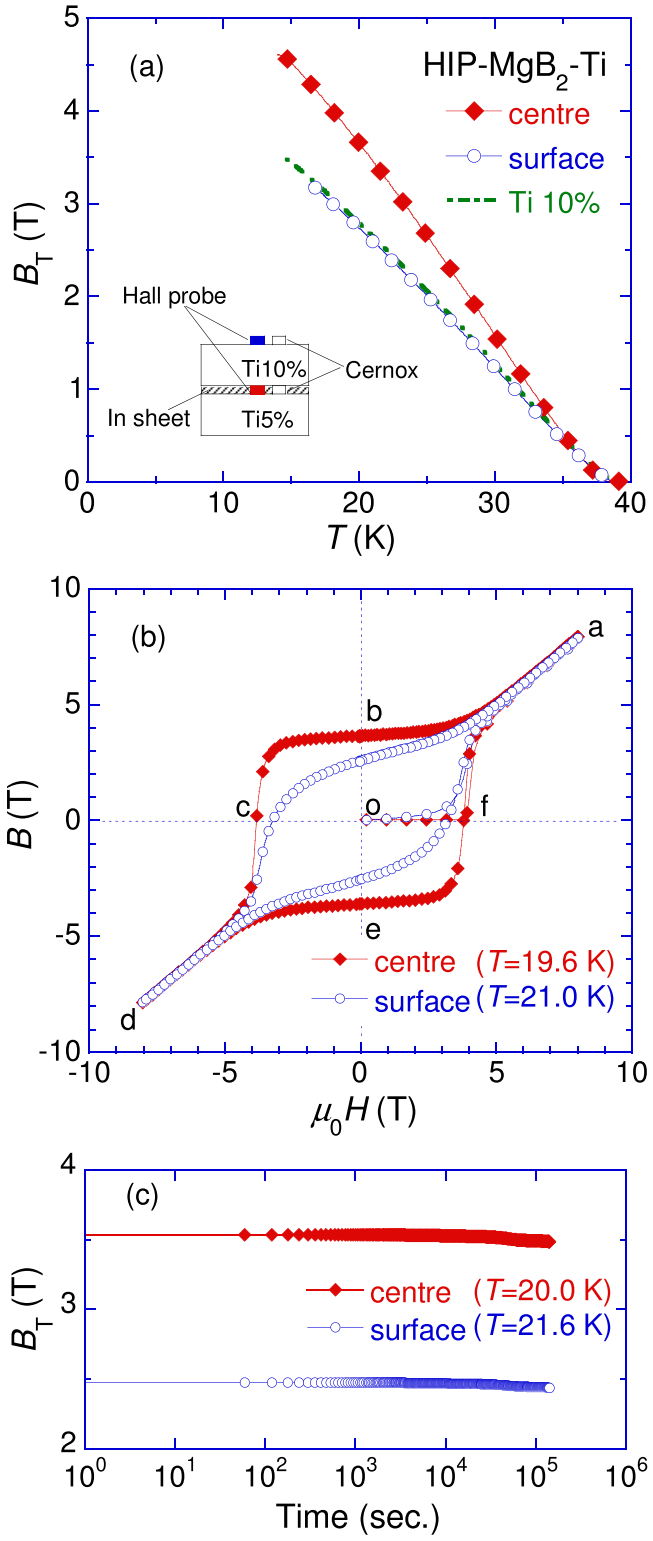

Figure 2. (a) Temperature dependence of the trapped magnetic field at the centre and top surface positions for the doubly stacked bulks consisting of Ti5% (lower) and Ti10% (upper) bulks. The configuration is schematically shown in the inset. (b) Magnetic hysteresis loop of the stacked bulk at 19.6 K for the centre and at 21.0 K for the surface positions. (c) Time dependence of the trapped field at 20.0 K for the centre and at 21.6 K for the surface positions.

can be realized between the bulks and in the hollow of cylindrical bulk.

Figure 2(b) shows the magnetic hysteresis curves at $T = 19.6$ K for the centre and at 21.0 K for the surface of the stacked bulks, respectively, which were taken after ZFC. The shape of the hysteresis loop of the centre position is nearly square, but that of the surface is rather round-shaped, which is caused by the demagnetization effect. The magnetization process at the centre position is as follows. The first branch from the applied magnetic field of $\mu_0 H = 0$ T to 8 T (o →a) in the first quadrant represents the first magnetization. The vortices start to reach the centre of bulk at about $\mu_0 H = 3.8$ T, and then the flux density increases with increasing magnetic field up to 8 T. Subsequently, the magnetic field is swept from 8 to –8 T (a → b → c → d). The remanent magnetic flux density of 3.6 T at $\mu_0 H = 0$ T (point b) is exactly the trapped magnetic field, and then the internal magnetic field reaches zero at $\mu_0 H = -3.9$ T (point c), which is the coercive force. The magnetic field begins to penetrate into the bulk centre again, and the inverse magnetization increases with increasing inverse magnetic field (c → d). The magnetization curve from $\mu_0 H = -8$ T to 8 T (d → e →f →a) is in line symmetry with the d-a line. Finally, as the magnetic field is ramped down to 0 T, the magnetization curve traces the initial a → b curve. The fact that the remanent magnetic flux density is nearly comparable with the absolute value of the coercive force demonstrates that the MgB_2 bulk magnet is an excellent hard magnet. Afterwards, we measured the time dependence of the trapped field to monitor the reduction in B_T due to vortex creep at the centre ($T = 20.0$ K) and at the surface positions ($T = 21.6$ K), respectively, as shown in figure 2(c). The initial B_T of 3.54 T (2.47 T) at $t = 0$ s, which is defined by the end time of the magnetising sweep, decreases to 3.48 T (2.43 T) at $t = 1.44 \times 10^5$ s (40 h) at the centre (surface) position. The creep for both positions is estimated to be approximately 2% for 40 h, which is small enough to use the bulk as a quasi-permanent magnet.

Figure 3 shows the critical current density, $J_c(\mu_0 H)$, as a function of the applied magnetic field, $\mu_0 H$, for the pristine and the Ti-doped samples at 10 and 20 K, in which some data points affected by flux jumps are not plotted. J_c of the pristine sample decreases strongly with increasing field; in particular, a rapid decrease is observed under fields higher than 4 T at 20 K. The irreversibility field, $\mu_0 H_{irr}$, is about 4.4 T for the pristine sample at 20 K, where $\mu_0 H_{irr}$ is defined as the magnetic field, for which $J_c = 10$ A cm^{-2}. Ti doping enhances the $J_c(\mu_0 H)$ values significantly in magnetic fields. The J_c of 4.0×10^3 A cm^{-2} for the pristine sample is enhanced to $1.6–1.8 \times 10^4$ A cm^{-2} for the Ti-doped samples at 20 K under a field of 3 T. Furthermore, the irreversibility field, $\mu_0 H_{irr}$, for the Ti-doped samples clearly exceeds 5 T at 20 K. On the other hand, the J_c value in the self-field, $J_c(0)$, is not improved so much by Ti doping. These results are summarized in the inset of figure 3, in which the normalized J_c value, $J_{c,x}/J_{c,x=0}$, is plotted as a function of Ti content, x, at each indicated magnetic field. Here, $J_{c,x}$ and $J_{c,x=0}$ are the J_c of the Ti-doped and the pristine samples, respectively. The magnitude of the

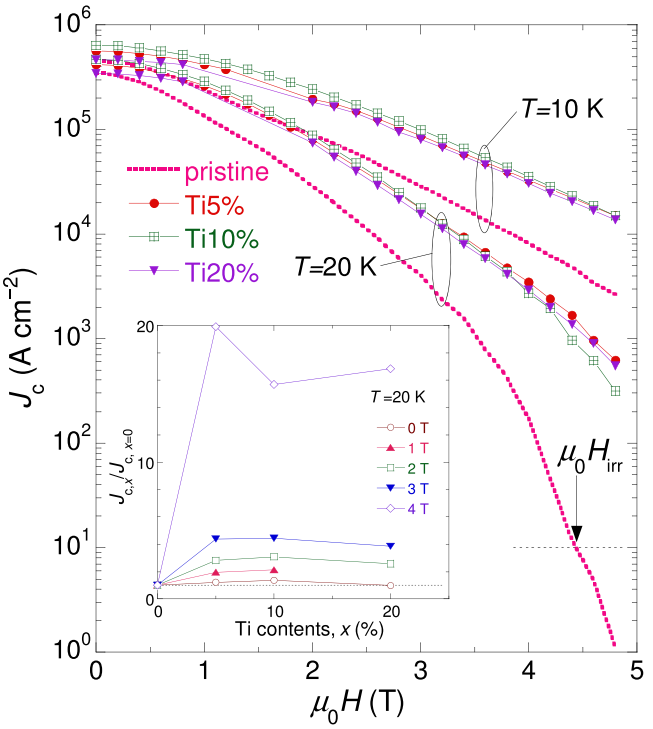

Figure 3. Magnetic-field dependence of the critical current density, $J_c(\mu_0 H)$, at 10 K and 20 K for the pristine and three Ti-doped MgB_2 bulks. The inset shows the normalized J_c value, $J_{c,x}/J_{c,x=0}$, of the Ti-doped samples as functions of Ti content and magnetic field. Here, $J_{c,x}$ and $J_{c,x=0}$ are the J_c of the Ti-doped and the pristine samples, respectively.

J_c enhancement evidently increases with increasing magnetic field, and a slight peak is observed for the Ti content of 10%, except for 4 T, which indicates that 10% is the optimal doping level. In a previous report [18], $J_c(0)$ at 20 K was increased from $\sim 2 \times 10^3$ A cm^{-2} in the non-doped sample to $\sim 1 \times 10^6$ A cm^{-2} in the Ti10% doped sample; however, the $J_c(\mu_0 H)$ of the latter sample started to decay steeply above 3 T and reached 10 A cm^{-2} at about 4 T. As a result, the reported $\mu_0 H_{irr}$ value is lower than that of the present non-doped bulk. At 10 K, the J_c in the magnetic field is also enhanced by Ti doping, and the relationship between the magnitude of the J_c increase and the Ti contents is similar to that at 20 K. These results suggest that the Ti doping in the present study offers effective pinning centres in high fields.

Figure 4(a) shows the magnetic field dependence of the pinning force density, $F_p(\mu_0 H)$, for the pristine and the Ti10% doped samples at 10 and 20 K. The magnitude of the F_p value is clearly enhanced by Ti doping at each temperature, which means that the pinning centres are created by Ti doping. The peak value, F_p^{max}, of the Ti10% bulk is about twice that of the pristine bulk at both temperatures, and the magnetic field at the peak of 0.76 T (0.98 T) for the pristine sample is shifted to 1.1 T (1.5 T) for the Ti10% sample at 20 K (10 K). Although flux jumps wiped out the peak of F_p for both the Ti5% and Ti20% bulks, they also showed similar $F_p(\mu_0 H)$ behaviour (not shown here), and the highest F_p value is obtained for the Ti10% bulk. To determine the dominant pinning mechanism,

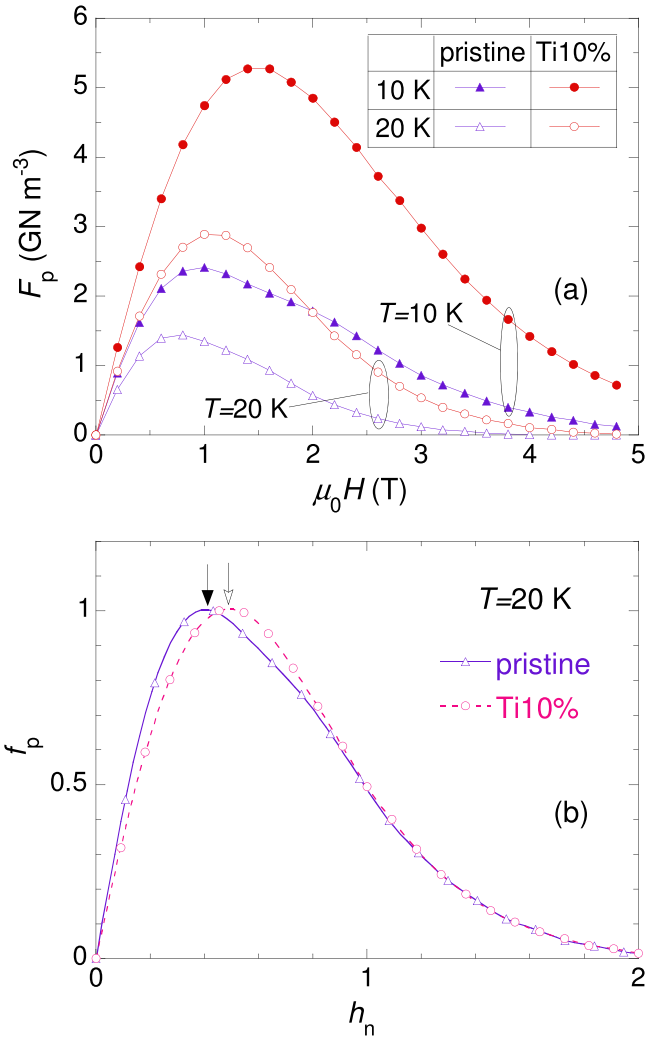

Figure 4. (a) Magnetic-field dependence of the pinning force density, $F_p(\mu_0 H)$, at 10 K and 20 K for the pristine and the Ti10%-doped MgB_2 bulk. (b) The reduced pinning force density f_p versus the reduced field h_n at 20 K proposed by Eisterer [29] (see text).

the $F_p(\mu_0 H)$ curve is usually analyzed by the scaling formula, $F_p \propto h_i^p(1-h_i)^q$, where h_i is the reduced field, $h_i = \mu_0 H/\mu_0 H_{irr}$, and the exponents p and q are characteristics for the dominant pinning mechanism [27]. For instance, $p = 1/2$ and $q = 2$ are predicted to be for grain boundary pinning and $p = 1$ and $q = 2$ for normal core point pinning. This procedure requires the $\mu_0 H_{irr}$ value; however, for the present Ti-doped samples, this is higher than 5 T and cannot be determined experimentally, as shown in figure 3. In such a case, the $\mu_0 H_{irr}$ value is often estimated by the theoretical Kramer plot [28]. However, Eisterer pointed out that this procedure was not suitable for anisotropic materials like MgB_2, because the anisotropy strongly affects the Kramer plot, which results in underestimating the $\mu_0 H_{irr}$ value [29]. He proposed a modified scaling procedure, allowing the identification of the dominant pinning mechanism from the peak position in the f_p (h_n) curve without the $\mu_0 H_{irr}$ value. Here, $f_p(= F_p/F_p^{max})$ is the reduced pinning force density, $h_n(= \mu_0 H/\mu_0 H_n)$ is the reduced magnetic field, and $\mu_0 H_n$ is defined as the magnetic field at which F_p drops to half of its maximum, F_p^{max}, at magnetic fields above the peak magnetic field. Furthermore, the peak position almost independent of the anisotropy, γ, and the percolation threshold, p_{sh}, where p_{sh} is defined as the minimum fraction of the superconducting region for a continuous supercurrent path. The peak field $h_{n,peak}$, was calculated for the five typical pinning mechanisms with $\gamma = 4$ and $p_{sh} = 0.25$ [29]: (1) $h_{n,peak} = 0.34$ for normal surface pinning ($p = 1/2$, $q = 2$), (2) $h_{n,peak} = 0.47$ for normal point pinning ($p = 1$, $q = 2$), (3) $h_{n,peak} = 0.56$ for superconducting volume pinning ($p = 1$, $q = 1$), (4) $h_{n,peak} = 0.62$ for superconducting surface pinning ($p = 3/2$, $q = 1$), and (5) $h_{n,peak} = 0.65$ for superconducting point pinning ($p = 2$, $q = 1$). Figure 4(b) shows the $f_p(h_n)$ curve at 20 K for both pristine and Ti10% bulks. The peak field, $h_{n,peak}$, shifts from 0.41 for the pristine to 0.49 for the Ti10% bulk. The main pinning source in MgB_2 is well known to be the surface (grain boundaries). The $h_{n,peak}$ value of 0.41 for the pristine bulk indicates that the grain boundaries are the dominant pinning centres, although it is somewhat larger than the calculated value of 0.34. On the other hand, the dominant pinning sources for the Ti10% bulk should be the point-like normal cores, because the $h_{n,peak}$ value of 0.47 is almost the same as 0.49 calculated for the normal core pinning, and Ti doping does not introduce a weak superconducting region in the MgB_2 matrix, as discussed in the inset of figure 1(a). Consequently, the observed peak shift strongly suggests that the pinning mechanism is changed by Ti doping. Remembering that the scaling analysis for the pinning force density can determine only the single pinning mechanism, we can conclude that the grain boundary pinning and additional point pinning related to Ti doping are effective for the Ti doped bulk. The details of the pinning centres introduced by Ti doping are discussed below.

Figure 5(a) shows the x-ray diffraction (XRD) patterns for the pristine and Ti-doped samples used in this study [30]. The dominant phase is MgB_2, and impurity phases such as Ti and TiB_2 begin to appear with Ti doping even for the Ti5% sample, and the intensity of their peaks increases with increasing Ti content. Figure 5(b) shows the ratio of the peak intensity of impurities to that of the MgB_2 (101) plane. The impurity intensity ratio of Ti gradually increases from about 7% for the Ti5% bulk to 10% for the Ti20% bulk. On the other hand, the amount of the TiB_2 phase monotonically increases with increasing Ti content, and the impurity intensity ratio reaches 10% for the Ti20% bulk. Both normal conducting Ti and TiB_2 phases are expected to act as the vortex pinning centres.

We observed the microstructure and composition of the bulk surface by FE-EPMA. Figure 6 shows the secondary electron images for the three Ti-doped bulks. The dominant gray region is the MgB_2 matrix phase, which demonstrates that the dense and homogeneous structure is obtained by the HIP process, similar to the literature [17]. The bright parts, which are Ti, obviously increase with Ti content, and the dark parts, which represent cracks and voids, also increase simultaneously. We then analyzed the chemical composition of the

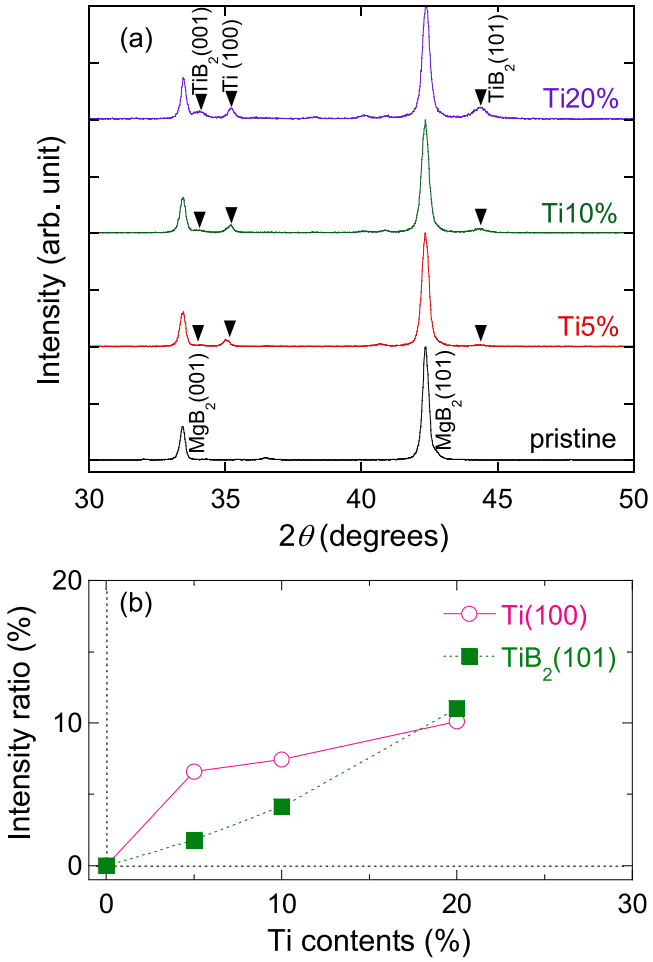

Figure 5. (a) Powder x-ray diffraction patterns taken at room temperature for the pristine and three Ti-doped MgB_2 bulks [30]. (b) Peak intensity ratio of impurity peak of Ti(100) and TiB_2(101) to the main peak of the MgB_2 (101).

bulks from the characteristic x-ray image for each element of Mg, Ti, and B, as shown in figures 7(b)–(d); the SE image of the same area is also shown in figure 7(a). The bright part represents each element. Mg and B disperse uniformly in the MgB_2 matrix phase. However, we can find some dark grey spots having a micrometric or nanometric dimension in the SE image; some of them are indicated by red arrows. They also appear as the dark and bright spots in the Mg and B maps, respectively, as indicated by red arrows, but not in the Ti map. Therefore, they are unreacted B or strongly Mg-deficient Mg-B particles; especially their nanometric particles could act as the point pinning centres. On the other hand, Ti is found as large precipitates, which correspond to bright regions in the SE image. Comparing chemical maps of Ti and B, B is found to be concentrated in the periphery of Ti; that is, B (thick bright line) surrounds Ti (large dark lump), as seen in figure 7(c). This thick region with micrometric dimension must be the polycrystalline TiB_2. The interfaces between nonsuperconducting TiB_2 and superconducting MgB_2 grains also possibly act as the point-like pinning centres. Therefore, these point-like pinning centres enhance both the J_c and $\mu_0 H_{irr}$ in high fields; this is supported by the analysis of the pinning force density. The microstructural analysis gives us evidence that the Ti-contained impurities, such as Ti and TiB_2, increase with increasing Ti content, which is consistent with the results of the XRD. It is noteworthy that the TiB_2 layer observed here is quite different from the lamellar TiB_2, which existed between the nanometre-size MgB_2 grains [19], which brings about the distinct pinning mechanism between the present and previous works. The typical size of Ti is estimated to be of the order of 10 μm. This is three orders of magnitude larger than $2\xi \sim 10$ nm [31] (ξ is the coherence length); therefore, the contribution of Ti on the vortex pinning is not so efficient.

4. Summary

We have studied the effects of Ti doping on the magnetic properties of MgB_2 bulks. The trapped magnetic field, B_T, critical current density, J_c, and microstructure were measured and observed using four $Mg_{1-x}Ti_xB_2$ (x = 0, 0.05, 0.1, and 0.2) bulks prepared by an *in-situ* hot isostatic pressing method. The important results are described below.

(i) The trapped magnetic field was enhanced by Ti doping. The B_T value of 3.6 T at 13 K was obtained for the Ti-doped bulk, which was 1.3 times larger than that of the pristine bulk. The $B_T(T)$ curves are almost independent of the Ti contents from x = 0.05–0.2.

(ii) The highest trapped field of 4.6 T was achieved at the centre of the doubly stacked bulks at 14.1 K, which was larger than that at the surface of the stacked bulks B_T = 3.6 T. A square-shaped magnetic hysteresis curve, in which the residual magnetism (trapped field) of 3.6 T and the absolute value of the coercive force of −3.9 T were comparable at 20 K, revealed that the MgB_2 bulk magnet was an excellent quasi-permanent magnet.

(iii) The trapped magnetic field at 20 K decayed only 2% over 40 h, which indicated high stability of the MgB_2 bulk magnet.

(iv) The pinning properties under magnetic field were improved by Ti doping. The J_c of 4.0×10^3 A cm^{-2} for the pristine sample was enhanced to that of $1.6–1.8 \times 10^4$ A cm^{-2} for the Ti doped samples at 20 K under a field of 3 T. The irreversibility field exceeded 5 T at 20 K for the Ti doped samples. The pinning force density, F_p, was enhanced by Ti doping and was maximized for Ti10%, which indicated that the pinning centres were introduced by Ti doping. The analysis of the F_p curve by Eisterer's scaling theory showed that the peak of the reduced F_p was shifted to a higher magnetic field by Ti-doping, which suggested that the pinning mechanism was changed; the point-like pinning became important, in addition to the grain boundary pinning.

(v) The unreacted B and strongly Mg-deficient Mg-B particles having nanometric dimensions was found. The Ti-contained impurities, such as Ti and TiB_2, increased with increasing Ti content. The nanometric B

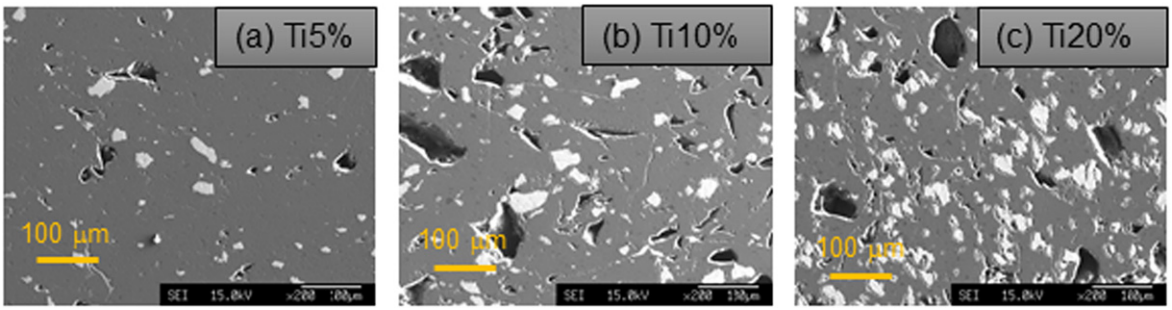

Figure 6. Secondary electron images for the Ti-doped bulks; (a) 5%, (b) 10%, and (c) 20%.

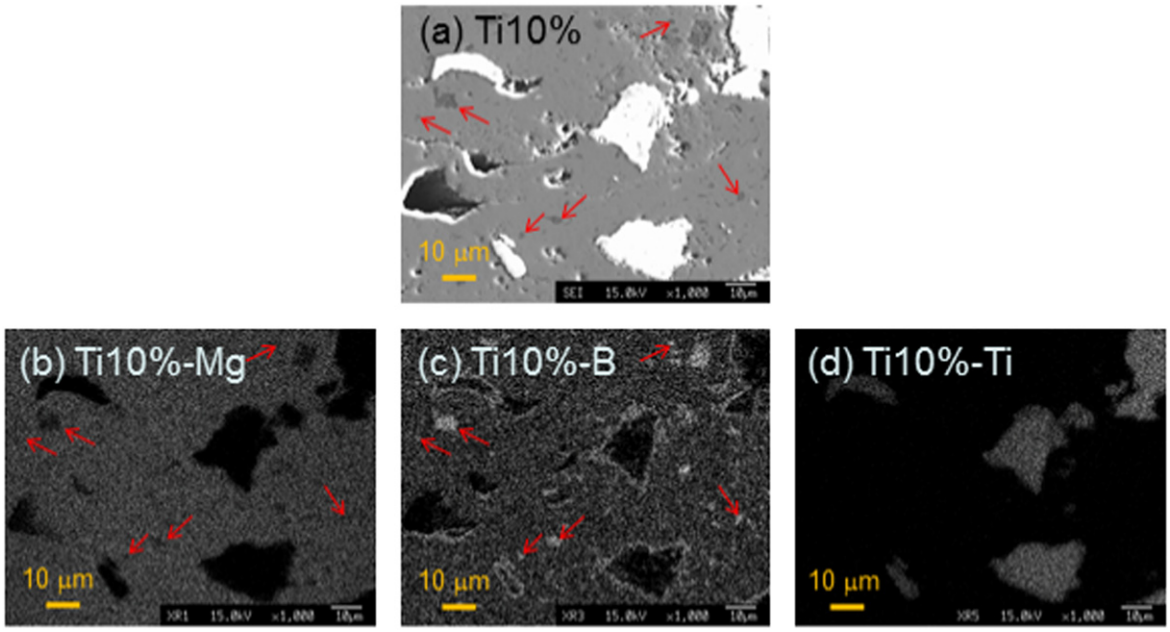

Figure 7. (a) Secondary electron image and characteristic x-ray images of (b) Mg, (c) B, and (d) Ti for the Ti10% bulk. The red arrows indicate the B or Mg-deficient Mg-B particles (see text).

and Mg-B particles and the interfaces between the TiB_2 and MgB_2 grains acted as a vortex pinning centre, and enhanced both J_c and B_T. On the other hand, the size of the Ti was about three orders of magnitude larger than the coherence length; thus the pinning effect of Ti was considered to be negligibly small.

Acknowledgments

We would like to acknowledge Dr H Teshima of Nippon Steel and Sumitomo Metal Corporation for his assistance in the production of the MgB_2 bulks using the HIP furnace and Miss M Sasaki and Mr K Nonaka of the Faculty of Engineering, Iwate University, for their help in the microstructure analysis using FE-EPMA. The authors also would like to thank Dr M D Ainslie of the University of Cambridge for his critical reading of this paper. This work was partly supported by JST A-STEP (AS242Z02673L), Hitachi Metals · Materials Science Foundation, and JSPS KAKENHI Grant Numbers 23560002, 15K04718, and 15K04646.

References

[1] Jin S, Tiefel T H, Sherwood R C, Davis M E, van Dover R B, Kammlott G W, Fastnacht R A and Keith H D 1988 *Appl. Phys. Lett.* **52** 2074–76
[2] Murakami M, Morita M, Doi K and Miyamoto K 1989 *Japan. J. Appl. Phys.* **28** 1189–94
[3] Nariki S, Sakai N and Murakami M 2005 *Supercond. Sci. Technol.* **18** S126–30
[4] Tomita M and Murakami M 2003 *Nature* **421** 517–20
[5] Durrell J H *et al* 2014 *Supercond. Sci. Technol.* **27** 082001
[6] Nagamatsu J, Nakagawa N, Muranaka T, Zenitani Y and Akimitsu J 2001 *Nature* **410** 63–64
[7] Kambara M, Babu N H, Sadki E S, Cooper J R, Minami H, Cardwell D A, Campbell A M and Inoue I H 2001 *Supercond. Sci. Technol.* **14** L5–7
[8] Larbalestier D C *et al* 2001 *Nature* **410** 186–9
[9] Murakami M and Yoo S I 2003 (http://semrl.t.u-tokyo.ac.jp/supercom/65/65_3.html) (in Japanese)

[10] Viznichenko R V, Kordyuk A A, Fuchs G, Nenkov K, Müller K H, Prikhna T A and Gawalek W 2003 *Appl. Phys. Lett.* **83** 4360–62
[11] Naito T, Sasaki T and Fujishiro H 2012 *Supercond. Sci. Technol.* **25** 095012
[12] Sasaki T, Naito T and Fujishiro H 2013 *Phys. Proc.* **45** 93–96
[13] Fuchs G, Häßler W, Nenkov K, Scheiter J, Perner O, Handstein A, Kanai T, Schultz L and Holzapfel B 2013 *Supercond. Sci. Technol.* **26** 122002
[14] Yamamoto A, Ishihara A, Tomita M and Kishio K 2014 *Appl. Phys. Lett.* **105** 032601
[15] Ohsaki H, Terao Y and Sekino M 2010 *J. Phys.: Conf. Ser.* **234** 032043
[16] Indrakanti S S, Nesterenko V F, Maple M B, Frederick N A, Yuhasz W H and Li S 2001 *Phil. Mag. Lett.* **81** 849–57
[17] Shields T C, Kawano K, Holdom D and Abell J S 2002 *Supercond. Sci. Technol.* **15** 202–5
[18] Zhao Y, Feng Y, Cheng C H, Zhou L, Wu Y, Machi T, Fudamoto Y, Koshizuka N and Murakami M 2001 *Appl. Phys. Lett.* **79** 1154–6
[19] Zhao Y, Huang D X, Feng Y, Cheng C H, Machi T, Koshizuka N and Murakami M 2002 *Appl. Phys. Lett.* **80** 1640–2
[20] Dou S X, Soltanian S, Horvat J, Wang X L, Zhou S H, Ionescu M, Liu H K, Munroe P and Tomsic M 2002 *Appl. Phys. Lett.* **81** 3419–21
[21] Takano Y, Takeya H, Fujii H, Kumakura H, Hatano T, Togano K, Kito H and Ihara H 2001 *Appl. Phys. Lett.* **78** 2914–6
[22] Prikhna T *et al* 2004 *Physica* C **402** 223–33
[23] Bean C P 1962 *Phys. Rev. Lett.* **8** 250–3
[24] Gyorgy E M, van Dover R B, Jackson K A, Schneemeyer L F and Waszczak J V 1989 *Appl. Phys. Lett.* **55** 283–5
[25] Fujishiro H, Naito T and Yoshida T 2014 *Supercond. Sci. Technol.* **27** 065019
[26] Zou J, Ainslie M D, Fujishiro H, Bhagurkar A G, Naito T, Babu N H, Fagnard J F, Vanderbemden P and Yamamoto A 2015 *Supercond. Sci. Technol.* **28** 075009
[27] Dew-Hughes D 1974 *Phil. Mag.* **30** 293–305
[28] Kramer E J 1973 *J. Appl. Phys.* **44** 1360–70
[29] Eisterer M 2008 *Phys. Rev.* B **77** 144524
[30] Yoshida T, Naito T and Fujishiro H 2015 *IEEE Trans. Appl. Supercond.* **25** 6801204
[31] Buzea C and Yamashita T 2001 *Supercond. Sci. Technol* **14** R115–46